

SWANN: Shuffling Weights in Crossbar Arrays for Enhanced DNN Accuracy in Deeply Scaled Technologies

Jeffrey Victor, Dong Eun Kim, Chunguang Wang, Kaushik Roy and Sumeet Gupta

Elmore Family School of Electrical and Computer Engineering, Purdue University

West Lafayette, IN 47907, USA

ABSTRACT

Deep neural network (DNN) accelerators employing crossbar arrays capable of in-memory computing (IMC) are highly promising for neural computing platforms. However, in deeply scaled technologies, interconnect resistance severely impairs IMC robustness, leading to a drop in the system accuracy. To address this problem, we propose SWANN - a technique based on shuffling weights in crossbar arrays which alleviates the detrimental effect of wire resistance on IMC. For 8T-SRAM-based 128x128 crossbar arrays in 7nm technology, SWANN enhances the accuracy from 47.78% to 83.5% for ResNet-20/CIFAR-10. We also show that SWANN can be used synergistically with Partial-Word-Line-Activation, further boosting the accuracy. Moreover, we evaluate the implications of SWANN for compact ferroelectric-transistor-based crossbar arrays. SWANN incurs minimal hardware overhead, with less than a 1% increase in energy consumption. Additionally, the latency and area overheads of SWANN are $\sim 1\%$ and $\sim 16\%$, respectively when 1 ADC is utilized per crossbar array.

KEYWORDS

In-Memory Computing, Interconnect, Matrix Vector Multiplication, Scaled technology nodes

1 INTRODUCTION

The remarkable success of deep neural networks (DNNs) in achieving super-human accuracy for several tasks has led to a surge in the exploration of DNN accelerators [1]. However, the current design approaches for DNN hardware involving von-Neumann platforms (such as central/graphic/tensor processing units-CPU/GPU/TPUs) are plagued by power-hungry and performance-limiting memory-processor transactions, which make them ill-suited for data-intensive DNN workloads. To address these limitations, in-memory computing (IMC) has emerged as a promising technique to integrate the storage and processing of data in a memory macro, alleviating the von-Neumann bottleneck [1].

Despite an immense promise of IMC, several challenges thwart its adoption in mainstream applications. A common IMC approach employs a crossbar memory array to compute matrix-vector multiplication (MVM) of activations and weights [1]. In an ideal scenario, the conductance of the memory element (storing the weight w) and the word-line voltage (representing the input

activation In) produce a current which encodes the scalar product of In and w . This current is naturally summed up on the sense-line (SL) to produce the MVM output. However, hardware non-idealities such as wire resistance, driver/sink resistance and device non-linearities/variations lead to a deviation of the SL current from its expected value. If large, this deviation can lead to computational errors, impairing DNN accuracy [1], [2].

This issue becomes even more critical in deeply scaled technologies. The importance of scalability of DNN accelerators is paramount to support the ever-increasing size of the DNN models for handling complex tasks. The technological advancements have led to scalable transistor topologies and non-volatile memory devices such as ferroelectric transistors (FeFETs) that are amenable to energy efficient IMC. However, interconnect scaling has been a major challenge [3], [4], [5]. Conventional copper (Cu) interconnects require barrier/liner layers to mitigate the issues associated with electromigration [4]. However, these layers do not scale well, thereby reducing the percentage of Cu as technology is scaled. This not only reduces the active area for current conduction, but also leads to an increase in sidewall scattering, increasing the interconnect resistivity (*not just resistance*) [3]. This issue is particularly severe for IMC since the wires in the crossbar array need to carry the accumulated currents of multiple memory cells, leading to large IR drops and significant computational errors.

Recognizing the significance of this issue, several techniques are being explored at the technology [4], [5] as well as design levels [6], [7], [8], [9], [10], [11]. For the former, alternate materials and processes for interconnects are being investigated, each with its own pros and cons [4], [5]. To complement these, several circuit design and algorithmic innovations promise to further enhance IMC robustness. These include enhancing the sparsity [8], [9], redistributing the weights [11], partial word-line activation [10] and hardware-aware training [6], [7]. While promising, these solutions have their own costs (details later). Further, most of these approaches have been analyzed for technologies in which the wire resistance is small, and the associated non-idealities are fairly manageable. While the scalability of these techniques needs further analysis, at the same time, there is a need for new approaches that effectively mitigate the detrimental effect of the wire resistance on IMC robustness and DNN accuracy in deeply scaled technologies.

In this work, we address this need by proposing a new technique based on shuffling weights in crossbar arrays for enhancing DNN accuracy, or SWANN. Our approach re-maps weights in the

crossbar arrays to mitigate the effect of wire resistances on IMC robustness. SWANN offers a training-free approach with minimal hardware overheads. Our key contributions are as follows:

- We propose SWANN which re-maps the weights in the crossbar arrays in such a way that the IR drops in the wire resistance is significantly reduced, thereby achieving high DNN accuracy in the presence of hardware non-idealities.
- We establish the efficacy of SWANN in deeply scaled technologies (7nm node) by analyzing 8T-SRAM and FeFET-based crossbar arrays.
- We show the synergy between SWANN with partial wordline activation or PWA (used to manage analog-to-digital converter (ADC) costs in IMC macros).
- We analyze the hardware implications of SWANN which requires dynamic activation re-mapping along with weight re-mapping to maintain the MVM functionality. We show that the design overheads of SWANN are minimal.

2 RELATED WORK

Several works [7-12] have explored solutions to mitigate the effect of hardware non-idealities that stem from parasitic resistances, device non-linearities and process variations. The works in [6], [7] have shown the efficacy of training DNNs including the device variations and wire resistance to improve their inference accuracy. However, these studies primarily focus on small datasets and networks (limited to 2 layers). The authors in [8] mitigated hardware non-idealities by re-training the network while limiting the output current range. While promising, these works [6-8] incur the cost of re-training the DNN.

Several other works have explored training-free strategies to counter non-idealities. In [9] and [11], crossbar columns are rearranged to position high current-producing or accuracy-critical columns closer to the drivers, thereby reducing non-idealities. [9] Another work in [10] utilizes partial wordline activation (PWA) to improve the inference accuracy by reducing the SL current. PWA asserts only a subset of WLS in one cycle, trading off inference accuracy with parallelism. In addition to mitigating non-idealities, it reduces the overheads of ADCs.

The works discussed above span technology nodes from 45nm to 65 nm, with wire resistance ranging from 2 Ω to 10 Ω per bitcell. However, in deeply-scaled nodes such as 7 nm, the wire resistance can increase up to 20 Ω per bitcell [2], [3], significantly impairing DNN accuracy. Hence, the efficacy of the techniques proposed in [7-12] need further evaluation for deeply-scaled technologies.

Recently, Wang et.al in [2] examined non-idealities in highly-scaled (7nm) technology nodes for DNN inference. This work showed that gate-input design i.e. applying the inputs on the gate of FeFETs or the access transistors of SRAMs (rather than on the drain) reduces the impact of parasitic resistances in crossbar arrays.

For a further improvement in DNN accuracy in deeply-scaled technology nodes, we propose SWANN which targets the mitigation of interconnect-induced non-idealities in crossbar

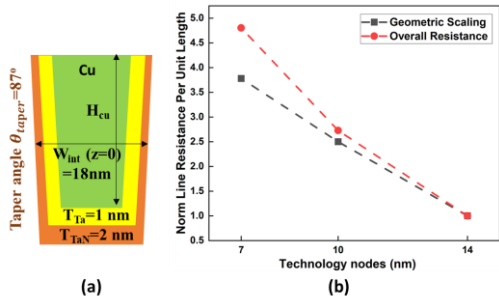


Fig. 1 (a) Interconnect Structure (b) Normalized Line Resistance per unit length across nodes

arrays. Our technique complements some of the aforementioned solutions such as gate-input design and PWA (discussed later) and may be used in conjunction with other prior approaches.

3 CROSSBAR ARRAY ANALYSIS AT 7 nm TECHNOLOGY NODE

Before we present SWANN, we analyze the implications of IMC in crossbar arrays at the 7nm technology node in this section to lay the groundwork for the rest of the paper. We discuss the increasing impact of interconnect resistance with technology scaling and illustrate its impact on the IMC robustness.

3.1 Interconnect Modeling and Analysis

Fig. 1 (a) shows the cross-section of the interconnect from [3] that we utilize for our analysis in this work. The active current conducting portion is composed of copper (Cu), which is surrounded by Ta liner and TaN barrier. In state-of-the-art technologies, 2nm Ta liner and 2nm TaN barrier is utilized [3]. However, scaling the liner to 1nm is being explored to increase the cross-sectional area of Cu for higher conductance [3]. In this work,

TABLE I
Device & Interconnect Parameters

ρ_{bulk}	0.0172
ρ_{Ta}	2
ρ_{TaN}	3
<i>Grain-boundary reflection coefficient</i>	0.135
<i>Electron mean free path [nm]</i>	40
<i>FE Thickness [nm]</i>	7
<i>Saturated Polarization [$\mu\text{C}/\text{cm}^2$]</i>	30
<i>Remanent Polarization [$\mu\text{C}/\text{cm}^2$]</i>	27
<i>FE Relative Permittivity</i>	22
<i>Coercive Electric Field [MV/cm]</i>	2.4
<i>Fin Pitch (FP)</i>	27 nm
<i>Gate Pitch (GP)</i>	54 nm
<i>Metal Pitch (MP)</i>	36 nm
<i>WL Voltage</i>	0.7 V
<i>BL Voltage</i>	0.25 V

we utilize the scaled liner design with 1nm Ta and 2nm TaN. We assume 50% sidewall coverage and a sidewall taper angle of 87° , based on [3]. It may be noted that for the state-of-the-art interconnects (with 2nm liner), the interconnect-related issues discussed later will be aggravated and the benefits of the proposed SWANN technique is expected to be even more significant.

To model the interconnects, we include the sidewall and grain-boundary (GB) scattering based on [12] and [13], respectively. For the 7nm technology node, we use the interconnect width (corresponding to M1-M3) to be 18nm and the pitch of 36nm. We build 3D interconnect models in COMSOL incorporating sidewall and GB scattering (parameters summarized in Table I) to analyze the structures in Fig. 1 (a).

Based on our models, we observe that the line resistance increases by 4.8x as we scale the technology from the 14 nm to 7 nm (Fig. 1b). This includes the effect of geometry scaling as well as increase in resistivity (ρ_{Cu}) due to higher sidewall scattering. [4], [14]. From our models, we obtain the values for the line resistance to be $182 \Omega/\mu\text{m}$ and via resistance to be 78Ω . These values are in good agreement with prior works [3], [14]. The line resistance also matches well with an IBM technology [4].

3.2 Simulation Framework for the Analysis of Interconnect-induced Non-Idealities and DNN Accuracy

In this section, we analyze crossbar arrays utilizing 8T-SRAM and FeFET designs [2] (Fig. 2 (a)). For 8T SRAMs, we utilize the predictive technology models (PTM) corresponding to 7 nm low standby power (LSTP) FinFETs [15]. For FeFETs, we utilize the model in [16] based on Miller’s multi-domain equations for the ferroelectrics (emulating the Preisach model). We couple the Miller’s model with 7nm PTM models to obtain the polarization-dependent device characteristics [17]. The parameters for the devices are summarized in Table I.

We design the 8T SRAM and FeFET bit-cells considering gate-input configuration and draw their layouts (Fig. 2) based on the metal-pitch and gate-pitch values for 7nm Intel process [18]. We consider a bit-slice of 1 in each bit-cell and input bit-stream = 1. The conductance values for various input (In) and weight bit (w) combinations (obtained from our models) are provided in Table II. We observe that compared to FeFETs, SRAMs offer higher ratio of conductance for the ON ($In=1$ and $w=1$) and OFF ($In=0$ or $w=0$) bit-cells, while FeFETs offer a more compact bit-cell footprint (half the cell height). As we will discuss later, both these factors play an important role in IMC. Based on these designs, we utilize the GENIEX framework [1] to study the effect of crossbar non-idealities on DNN inference accuracy at the 7nm technology node.

TABLE II

Device Conductances for Different Input and Weight Combinations

	$In = 1$ $W = 1$	$In = 1$ $W = 0$	$In = 0$ $W = 1$	$In = 0$ $W = 0$
SRAM(S)	$1.6 * 10^{-5}$	$4.7 * 10^{-12}$	$6.6 * 10^{-12}$	$2.2 * 10^{-12}$
FeFET(S)	$1.6 * 10^{-5}$	$2.50 * 10^{-7}$	$4.3 * 10^{-8}$	$2.0 * 10^{-10}$

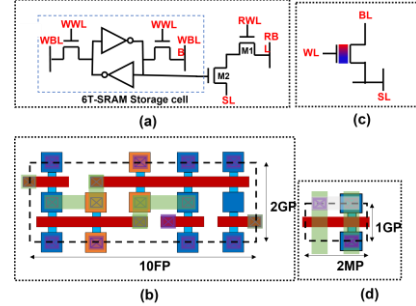


Fig. 2 (a) 8T-SRAM and its (b) layout. (c) FeFET and its (d) layout

3.3 Non-idealities in Crossbar Arrays

Fig. 3 shows a typical crossbar array along with the parasitic resistances (wire resistance R_W , driver resistance R_D and sink resistance R_S). As the current-carrying lines (RBL/BL and SL) are routed along the columns, their length and therefore, R_W is determined by the layout height of the cells and the number of cells in a column. The IR drop in the parasitic resistances (R_W , R_S and R_D) lead to deviation of the output current from its expected values, which can result in computational errors. Due to high R_W at the 7nm technology node (discussed in the previous sub-section), these deviations are large, leading to a large impact on DNN accuracy. Our analysis shows that the impact of R_W is twofold. First, the drain voltage of the transistors is reduced. Second, the source voltage is increased (leading to source degeneration). While both contribute in reducing the cell current, the latter effect is more critical in SRAMs and FeFETs as the increase in source voltage reduces both the gate-to-source voltage (V_{GS}) and drain-to-source voltage (V_{DS}).

Moreover, due to the distributed nature of R_W in a column, the deviation in the output current depends on the distribution of the weights and inputs in a column. For instance, consider two cells which are ON (i.e. with $In=1$ and $w=1$): Cell A is closer to the ADC (bottom of the array in Fig. 3) and farther away from the BL/RBL driver than Cell B. During IMC, the source voltage of Cell A is closer to 0 (the ideal value), but its drain voltage is lower than Cell B. As mentioned before, the effect of source degeneration is more dominant, and hence, the deviation of current in Cell A is lower than Cell B. The standard weight mapping leads to different input/weight distributions in crossbar arrays, resulting in range of output currents for the same expected MVM product.

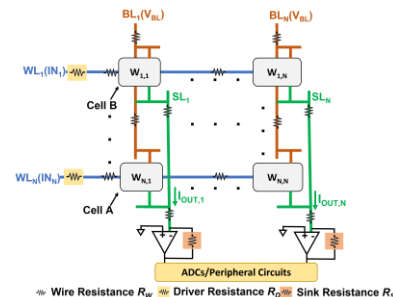


Fig. 3 Crossbar array in gate-input configuration with wire-resistances and other parasitic resistances.

In other words, the final output current depends on the distribution of the weights and inputs in a column, the parasitic resistances and array size (in addition to other device-level attributes). Our simulations show that for a 7nm technology node, high R_W leads to significant deviations of the output current causing the DNN accuracy to drop from the software accuracy of 92.8% to 47.78% (88.8%) for 8T-SRAMs and 84.85% (91.63%) for FeFETs in a 128x128 (64x64) array. Note, SRAMs show a higher accuracy drop than FeFETs as their cell height, and therefore, R_W is larger.

4 SWANN: Shuffling weights to reduce wire-induced non-idealities

4.1 The key idea

The discussions in the previous section suggest that due to IR drops on the parasitic resistances and the consequent source degeneration, an 8T SRAM or FeFET bit-cell farther away from the ADC exhibits a larger reduction in its current (encoding the scalar product of its weight and input) than the one closer to the ADC. Hence, we propose to reduce the deviation of the dot product (SL current) from its expected value by re-mapping the weights in the array such that the bit-cells storing $w=1$ (low resistance state or LRS) are agglomerated in the lower rows (closer to the ADC), while the bit-cells with $w=0$ (high resistance state or HRS) are in the upper rows. Interestingly, the proposed technique not only increases the current of the ON bit-cells ($w=1$ and $I_n=1$) towards the expected values (by lowering the effect of IR drops), it also reduces the current in the bit-cells storing 0 by inducing a stronger source degeneration. Note that bit-cells with $w=0$ produce non-zero currents due to finite resistance of the HRS. This aggravates the non-ideal effects in crossbar arrays. SWANN reduces the current in such bit-cells, thereby further mitigating the non-idealities. It is also noteworthy that when the input (I_n) = 0, the LRS bit-cells also produce non-zero current due to leakage. However, these leakage currents are much smaller than the currents corresponding to HRS of the bit-cell. Hence, reducing the current for $w=0$ via the proposed technique has a more dominant and desirable effect compared to the leakage increase in the cells storing 1. Thus, SWANN achieves an increase in the ON current and the reduction in the HRS currents at an insignificant cost of leakage increase.

To maintain the correct MVM functionality, the proposed weight re-mapping must be accompanied by re-mapping of the input activations. Since the inputs are applied along the rows of a

crossbar array, the columns cannot be re-arranged independently. Therefore, we propose to re-arrange the weights by analyzing the sum of weights stored in a row (called the row-sum) and mapping the rows with the largest row-sum to the bottom of the crossbar array. In this way, the columns of the crossbar array are expected to have a large number of LRS bit-cells closer to the ADC.

To achieve this, we follow the following process (Fig. 4). First, we compute the row-sum of each row. Second, the row-sum of each row is concatenated into a vector and sorted in ascending order. In this step, we use an additional vector called the tracking vector which stores the position of each row in the sorted row-sum vector. For example, if the second row has the highest sum out of all 64 rows, the tracking vector updates its second entry as 64. Essentially, the tracking vector stores the address of the destination that each row should be swapped into while deploying the weights in the crossbar array. These two steps are performed in software *before* mapping the weights in the DNN accelerator incurring a one-time cost. Next, the re-arranged weights are deployed in the crossbar arrays. The corresponding inputs are dynamically swapped according to the tracking vector in the hardware. We will discuss the hardware implications of this later. After this step, the crossbar arrays have most of the LRS bit-cells in the bottom rows.

In this work, we re-map the rows for each crossbar array independently. Alternatively, we could perform this swap at a higher granularity by taking row-sums across multiple crossbars and then performing weight re-mapping based on a common tracking vector. This would reduce the hardware overhead and is expected to simplify dynamic re-mapping of the inputs. However, this would, in general, reduce the effectiveness of SWANN in mitigating the effect of non-idealities (which needs to be analyzed in the future). In this work, we focus on independent re-mapping for each crossbar array, showing its effectiveness in enhancing DNN accuracy and analyzing its hardware costs.

4.2 Complementing Partial Wordline Activation (PWA) with SWANN

PWA is a common technique used for IMC in crossbar arrays, in which only a subset of rows is activated in a single cycle. Thus, the MVM computation is broken down in multiple steps. This helps in mitigating two important issues. First, the range of the SL current is reduced, mitigating the IR drops and the associated non-idealities [10]. Second, this relaxes the bit-precision requirements for the

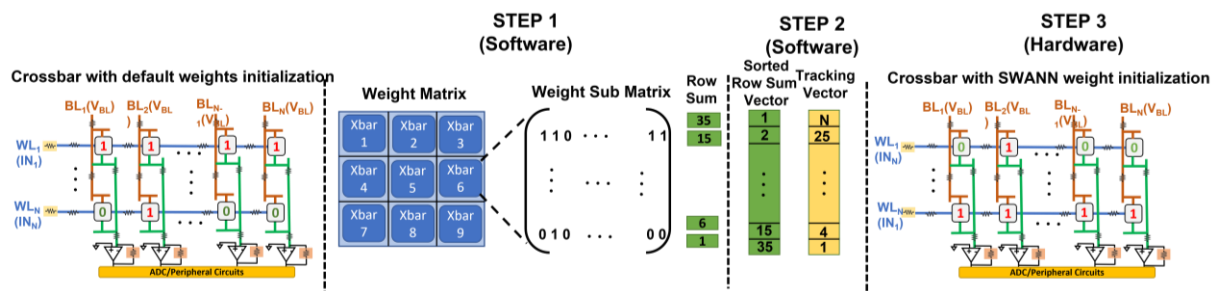


Fig. 4 Three Steps of the SWANN technique

ADCs, significantly reducing their energy and area costs (which are known to be dominant in IMC macros [19], [20]).

In standard methods (where the weight and input distribution is arbitrary), each cycle of PWA involves asserting consecutive rows concurrently. For example, for a crossbar of size $N \times N$ grouped into M groups the first N/M rows are asserted in the first cycle, second N/M rows in the second cycle and so on. Interestingly, in SWANN, the distribution of cells storing weight bit = 1 is concentrated towards the bottom of the array due to weight agglomeration. Thus, if standard PWA is naively applied with SWANN, the current in the later cycle is expected to be much more, which could reduce the effectiveness of PWA. Interestingly, since the weight pattern is known in SWANN, we can synergize the beneficial effects of PWA and SWANN. For this, instead of asserting consecutive rows in a single cycle, we propose activating the rows in a distributed fashion in a SWANN crossbar. For example, in the crossbar with N rows and M groups. The i th group asserted in the i th cycle consists of rows i , $i+N/M$, $i+2N/M$, etc. We will refer to this approach as Distributed PWA (DPWA). By grouping WLS in such a distributed fashion, we distribute the high row-sum rows among different groups. Thus, in each DPWA cycle, the number of cells producing scalar output of 1 is expected to reduce compared to a naïve PWA+SWANN, thereby further mitigating the effect of non-idealities.

5 RESULTS AND DISCUSSION

In this section, we quantify the efficacy of SWANN in boosting the inference accuracy and analyze the associated hardware overheads. We analyze ResNet-20 for CIFAR-10 dataset and compare the proposed SWANN technique with the baseline (in which standard weight mapping is used).

5.1 Effect of SWANN on Accuracy

The effect of SWANN on 64x64 and 128x128 8T SRAM arrays is shown in Fig. 5 (a). For the baseline design, 64x64 SRAM crossbar arrays yield an inference accuracy quite close to the software baseline. However, as we increase array size to 128x128, the inference accuracy drops by 41% due to higher wire resistance. On applying the proposed SWANN technique, we observe the inference accuracy increases (by 2.85%) from 88.8% to 91.65% in the 64x64 array while it increases (by 35.72%) from 47.78% to 83.5% in the 128x128 array. In other words, by reducing the impact of interconnect-induced non-idealities, SWANN enables the design of *larger* crossbar arrays in deeply scaled technologies, which can reduce the peripheral circuit overhead.

To gain further insights into SWANN, we show its implications for FeFET based arrays (Fig. 5 (b)). On applying SWANN, we observe the inference accuracy increases from 84.85% to 87.53% in 128x128 FeFET array. From Fig. 5 (b), we can observe that SWANN enables a more graceful decline in accuracy for the 256x256 FeFET array, compared to the sharp decrease observed in baseline designs.

5.2 Analysis of SWANN with PWA/DPWA

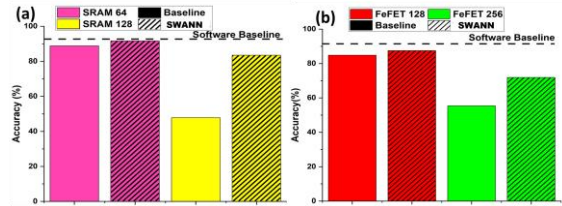


Fig. 5 Effect of SWANN on Varying Array size of (a) SRAM and (b) FeFET

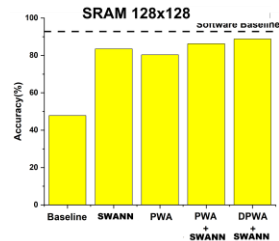


Fig. 6 Comparison of Accuracy using SWANN with PWA/DPWA on 128x128 8T-SRAM array

Next, we show the effect of combining PWA/DPWA with SWANN in Fig. 6. We perform this analysis for 128x128 8T SRAM array and fix the number of activated WLS per cycle to 64 in each of the PWA/DPWA cycles.

First, we observe that applying SWANN to a 128x128 SRAM improves accuracy to 83.5% while applying PWA increases accuracy to 80.34%. With PWA + SWANN, accuracy increases to 86.25% while the proposed DPWA+ SWANN, accuracy increases to 88.83%. Higher accuracy in DPWA+SWANN compared to PWA+SWANN establishes the synergy between DPWA and SWANN discussed in Section 4.2.

5.3 Overhead Analysis

In this section, we estimate the overheads of SWANN for ResNet-20 and CIFAR-10 considering 128x128 SRAM and FeFET arrays using SAMBA (Fig. 7) [20], a DNN inference accelerator with a spatial architecture similar to ISAAC [19]. It is important to note that while SAMBA suggests multiple data-movement optimizations, we avoid them here to focus solely on evaluating the impact of SWANN on a generic weight-stationary architecture. While re-mapping weights incurs a one-time cost that can be handled before runtime, re-mapping inputs is dynamic at run-time.

Recall that typically, inputs are shared across multiple crossbars in baseline design. In SWANN, each crossbar requires its own input re-mapping. Hence, we utilize the tracking vectors as a Look-up-Tables (LUTs) to make multiple copies of the input for each crossbar and write it into buffers. Then, these buffered input values are applied to the crossbar as WL voltages.

We analyze energy, latency and area overheads of SWANN for two scenarios in Table III: 1 ADC per crossbar and 16 ADCs per crossbar [19], [21]. Multiple DNN accelerators, such as ISAAC [19], utilize only one ADC per crossbar, as ADCs are the most dominant energy-consuming component and a substantial area-

Table III
Energy/Latency/Area Overheads for SWANN

ADCs per Xbar	Array	Latency Overhead	Energy Overhead	Area Overhead
1	SRAM 128x128	0.7%	0.2%	16.09%
1	FeFET 128x128	1.1%	0.5%	1.89%
16	SRAM 128x128	11.5%	0.3%	3.16%
16	FeFET 128x128	17.6%	0.7%	0.34%

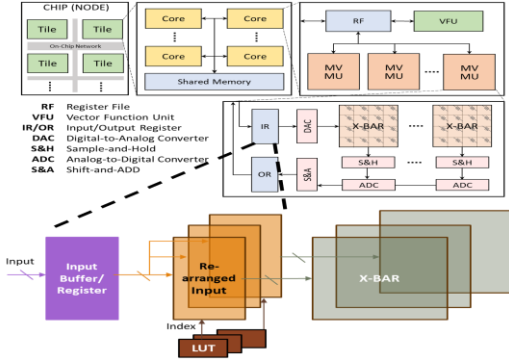


Fig. 7. SAMBA Architecture with Input Re-mapping

consuming component of MVM macros [19]. Conversely, other accelerators, such as TAICHI [21], employ up to 16 ADCs per crossbar to enhance parallelism at the cost of additional energy and area [21]. Hence, we evaluate SWANN for different number of ADCs per crossbar array and analyze the associated overheads.

From Table III, it is evident that SWANN incurs minimal energy overhead at less than 1%. This is primarily due to the dominance of ADCs in energy consumption which reduces the energy cost of additional hardware needed in the SWANN design. When 1 ADC is used per crossbar array, SWANN incurs 1.1% latency cost. This is because the sharing of ADC amongst multiple columns in a crossbar array increases the overall latency (even for the baseline design), which reduces the latency overhead of additional circuitry required by SWANN. However, if 16 ADCs are used per crossbar array, the latency of the baseline design reduces, as a result of which the latency cost of SWANN increases to 17.6%. From Table III, we also observe that the area overhead is up to 16.09% (3.16%) for 1 (16) ADC per crossbar. As the number of ADCs per crossbar increase, they occupy a higher proportion of the accelerator’s area. This reduces the relative share of area associated with the extra circuits needed for SWANN.

6 CONCLUSION

We propose SWANN to mitigate interconnect-induced non-idealities and enhance DNN inference accuracy by re-mapping weights in the crossbar arrays. By sorting rows based on their row-sum, SWANN places most low-resistance state devices closest to the ADC, reducing wire resistance-induced source degeneration. Our analysis at 7nm demonstrates SWANN’s ability to improve the inference accuracy of 128x128 SRAM by 35.72% with respect to the baseline. For FeFETs, SWANN increases the accuracy of

128x128 FeFET from 84.85% to 87.53%. We also propose utilizing SWANN with distributed PWA, which enhances the accuracy by 41.05% with respect to the baseline for 128x128 SRAM based design. SWANN incurs minimal hardware overhead, with less than 1% increase in energy consumption. Additionally, the latency overhead of SWANN is about 1.1%, while the area overhead is ~16% when 1 ADC is used per crossbar array.

REFERENCES

- [1] Chakraborty, I. et al. 2020. GENIEx: A Generalized Approach to Emulating Non-Ideality in Memristive Xbars using Neural Networks. *2020 57th ACM/IEEE Design Automation Conference (DAC)* (2020), 1–6.
- [2] Wang, C. et al. Design Space Exploration and Comparative Evaluation of Memory Technologies for Synaptic Crossbar Arrays: Device-Circuit Non-Idealities and System Accuracy. *arXiv preprint arXiv: 2307.04261*.
- [3] Chen, X. et al. 2021. Modeling and Circuit Analysis of Interconnects with TaS₂ Barrier/Liner. *2021 Device Research Conference (DRC)* (2021), 1–2.
- [4] Bonilla, G. et al. 2020. Interconnect scaling challenges, and opportunities to enable system-level performance beyond 30 nm pitch. *2020 IEEE International Electron Devices Meeting (IEDM)* (2020), 20.4.1-20.4.4.
- [5] Brain, R. 2016. Interconnect scaling: Challenges and opportunities. *2016 IEEE International Electron Devices Meeting (IEDM)* (2016), 9.3.1-9.3.4.
- [6] Liu, B. et al. 2015. Vortex: Variation-aware training for memristor X-bar. *2015 52nd ACM/EDAC/IEEE Design Automation Conference (DAC)* (2015), 1–6.
- [7] Liu, B. et al. 2014. Reduction and IR-drop compensations techniques for reliable neuromorphic computing systems. *2014 IEEE/ACM International Conference on Computer-Aided Design (ICCAD)* (2014), 63–70.
- [8] Bhattacharjee, A. et al. 2022. NEAT: Nonlinearity Aware Training for Accurate, Energy-Efficient, and Robust Implementation of Neural Networks on 1T-1R Crossbars. *Trans. Comp.-Aided Des. Integ. Cir. Sys.* 41, 8 (Aug. 2022), 2625–2637.
- [9] Bhattacharjee, A. et al. 2022. Examining and Mitigating the Impact of Crossbar Non-Idealities for Accurate Implementation of Sparse Deep Neural Networks. *Proceedings of the 2022 Conference & Exhibition on Design, Automation & Test in Europe* (Leuven, BEL, 2022), 1119–1122.
- [10] Yi, W. et al. 2019. Effect of Device Variation on Mapping Binary Neural Network to Memristor Crossbar Array. *2019 Design, Automation & Test in Europe Conference & Exhibition (DATE)* (2019), 320–323.
- [11] Agrawal, A. et al. X-CHANGR: Changing Memristive Crossbar Mapping for Mitigating Line-Resistance Induced Accuracy Degradation in Deep Neural Networks. *arXiv preprint arXiv:1907.00285*.
- [12] E. H. Sondheimer. 1950. The Influence of a Transverse Magnetic Field on the Conductivity of Thin Metallic Films. (1950) *Phys. Rev.* 401-406.
- [13] A. F. Mayadas and M. Shatzkes. 1970. Electrical-Resistivity Model for Polycrystalline Films: the Case of Arbitrary Reflection at External Surfaces. *Phys. Rev. B* (1970) 1382-1389.
- [14] Huang, V. et al. 2020. Modeling and Benchmarking Back End Of The Line Technologies on Circuit Designs at Advanced Nodes. *2020 IEEE International Interconnect Technology Conference (IITC)* (2020), 37–39.
- [15] Clark, L.T. et al. 2016. ASAP7: A 7-nm finFET predictive process design kit. *Microelectronics Journal.* 53, (Jul. 2016), 105–115.
- [16] Saha, A.K. and Gupta, S.K. 2018. Modeling and Comparative Analysis of Hysteretic Ferroelectric and Anti-ferroelectric FETs. *2018 76th Device Research Conference (DRC)* (2018), 1–2.
- [17] K. Ni et al. 2018. In-Memory Computing Primitive for Sensor Data Fusion in 28 nm HKMG FeFET Technology, in *2018 IEEE International Electron Devices Meeting (IEDM)* (2018), 16.1.1-16.1.4.
- [18] https://en.wikipedia.org/wiki/7_nm_lithography_process: https://en.wikipedia.org/wiki/7_nm_lithography_process. Accessed: 2023-11-27.
- [19] Shafee, A. et al. 2016. ISAAC: A Convolutional Neural Network Accelerator with In-Situ Analog Arithmetic in Crossbars. *2016 ACM/IEEE 43rd Annual International Symposium on Computer Architecture (ISCA)* (2016), 14–26.
- [20] Kim, D.E. et al. 2023. SAMBA: Sparsity Aware In-Memory Computing Based Machine Learning Accelerator. *IEEE Transactions on Computers.* 72, 9 (2023), 2615–2627.
- [21] Wang, X. et al. 2022. TAICHI: A Tiled Architecture for In-Memory Computing and Heterogeneous Integration. *IEEE Transactions on Circuits and Systems II: Express Briefs.* 69, 2 (2022), 559–563.